

# Investigating the Performance of Coded GSIM DCSK Communication Systems over Multipath Rayleigh Fading Channel

Ali Jaber Al-Askery, Fadhil Sahib Hasan, and Ahmed A. Thabit

**Abstract**—Index modulation–based differential chaos shift keying (IM–DCSK) is a promising technique in wireless communication systems. Among all schemes, a Grouping Subcarrier Index Modulation DCSK (GSIM–DCSK) supports suit–coded modulation to improve bit error rate (BER) over a multipath Rayleigh fading channel, known as Coded GSIM–DCSK (CGSIM–DCSK) system. In the proposed method, all the index modulation bits are detected at the receiver side and then converted into a bipolar form to pass them through the channel decoder system along with the soft modulated bits. The results show that CGSIM–DCSK system with two schemes that are CGSIM–DCSK1 and CGSIM–DCSK2 are improved by the proposed coding techniques, with the LDPC code barely superior to the New Radio–Polar Code (NRPC). Furthermore, the performance of CGSIM–DCSK1 outperforms that of CGSIM–DCSK2 with lower information rate.

**Index Terms**—Grouping Subcarrier Index Modulation based DCSK, LDPC, NRPC, Multipath Rayleigh Fading Channel.

## I. INTRODUCTION

WIDEBAND non-periodic chaotic signals are used as carriers in chaotic communications, which offers advantages over spread-spectrum systems such as reducing multipath fading impact [1]. Differential Chaos Shift Keying (DCSK) is one of the chaos-based communication schemes that have been introduced in recent studies [2], [3]. The robustness of DCSK systems in multipath fading environments is noteworthy, as they require minimal synchronization of the receiver signal, non-coherent detection without needing the channel state of information, and the properties of wideband chaotic signals. Because of this, chaotic signal techniques hold great promise for improving wireless communication resilience in the face of multipath fading issues [4].

Extra information bits were transmitted in [5] by suggesting a new chaos modulation scheme that incorporates Code Index Modulation (CIM) and takes a fresh approach based on the Walsh code index. This improvement greatly expands the spectrum and increases the energy efficiency

of chaos modulation based on CIM. The paper assesses two CIM–enhanced systems, CIM–DCSK and CIM–Short Reference–DCSK (CIM–SR–DCSK), and uses simulations to demonstrate how well they perform in comparison to conventional chaos systems.

Nonbinary Low–Density Parity Check (LDPC) for Coded Modulation–DCSK (CM–DCSK) systems has been presented in [6], which uses nonbinary protograph codes over Galois Field (GF(M)) in place of conventional binary coding. By avoiding iterative decoding and utilizing soft information straight from non–coherent detectors for channel decoding, this method simplifies receiver structures. Two types of non–binary codes that show rates closer to system capacity than binary codes are validated by modified EXIT analysis. The simulation results show notable improvements in performance; in Rayleigh fading channels, 16–ary CM–DCSK achieves 1.8 dB advantage over binary equivalents at BER  $10^{-4}$ . CM–DCSK has up to 2.3 dB improvement over FM–BICM–DCSK in real–world WLAN UWB scenarios, highlighting its practical advantages.

Carrier–Time–Index–Modulation–DCSK (CTIM–DCSK) has been proposed in [7] to improve data transmission efficiency. The BER performance in Additive White Gaussian Noise (AWGN) and Rayleigh fading channels is enhanced by incorporating a receiver noise–reduction module and uses carrier and time indices to convey additional information bits. CTIM–DCSK is better suited for low–power Internet of Things applications like WLAN and WPAN because it has less complexity than a number of DCSK variants and offers higher data rates and spectral efficiencies.

To facilitate effective chaotic communication, Reference Modulated–DCSK (RM–DCSK) was proposed in [8], which doubles the achievable bit rates while maintaining the same level of decoding complexity by applying chaotic wavelets across alternating slots within each frame. It improves communication security over conventional DCSK. Utilizing the Gaussian approximation, the BER performance in AWGN channels is found to be superior to that of CDSK, DCSK, Frequency–Modulated DCSK, and High–Efficiency DCSK. Simulations validate that RM–DCSK always performs better than CDSK and can even outperform DCSK when certain conditions are met, like high spreading factors or specific  $E_b/N_0$  levels.

In order to maintain acceptable bit error rates in the

Manuscript received September 3, 2024; revised October 16, 2024. Date of publication December 9, 2024. Date of current version December 9, 2024. The associate editor prof. Adriana Lipovac has been coordinating the review of this manuscript and approved it for publication.

A. J. Al-Askery and A. A. Thabit are with the Department of Automation and Control Technical Engineering, Electrical Engineering Technical College, Middle Technical University, Baghdad, Iraq (e-mail: a.al-askery@mtu.edu.iq).

F. S. Hasan is with the Electrical Engineering Department, College of Engineering, Mustansiriyah University, Baghdad, Iraq.

Digital Object Identifier (DOI): 10.24138/jcomss-2024-0072

face of mutual interference, the performance of a co-existing Code Shifted-DCSK/Binary Phase-shift keying (CS-DCSK/BPSK) system in spread spectrum communication has been assessed in [9]. CS-DCSK/BPSK performs better than DCSK/BPSK in a variety of channel conditions with comparable levels of interference, according to a comparative analysis. Numerical simulations in close agreement with theoretical predictions confirm the minimal impact of CS-DCSK on BPSK and highlight the efficacy of CS-DCSK as a new interferer in synchronized and asynchronous scenarios, as indicated by analytical expressions for BER.

A new multi-carrier M-ary DCSK system with code index modulation, called CIMMC-M-DCSK, has been proposed in [10]. It uses M-DCSK modulation to increase data rates while simultaneously transmitting reference and information-bearing signals on each subcarrier using orthogonal sinusoidal carriers. Walsh codes are used to optimize energy utilization by encoding additional information bits on reference signals across all subcarriers. For CIMMC-M-DCSK in AWGN and multipath Rayleigh fading channels, analytical BER formulas are obtained. The system offers differentiated Quality of Service (QoS) based on data importance and improves BER performance with noise-reduction and hierarchical modulation schemes. Simulation results show the superiority of the system and validate theoretical predictions.

General Code-Shifted (GCS-DCSK) systems have been presented in [11] with a novel approach to improve their data rate efficiency. In addition to the conventional Walsh codes used in GCS-DCSK, CIM-CSDCSK carries extra bits via code index modulation. This scheme allows different Walsh codes chosen by an integer sequence derived from information symbols to modulate multiple signals carrying information. BER over AWGN channels is analytically derived and numerical simulations confirming the superiority of CIM-CSDCSK over GCS-DCSK are presented. By carrying more bits per transmitted symbol while maintaining the same resource constraints, the suggested scheme increases spectrum efficiency.

To improve the DCSK performance without depending on intricate channel code designs which are essential for short frame transmissions, an Iterative Receiver-DCSK (IR-DCSK) has been proposed in [12]. It presented a soft demapping method for non-coherent M-ary DCSK systems that can be adjusted to different channel conditions, such as fading amplitudes. For various channel models, BER analysis showed benefits over non IR-DCSK, and achievable rate curves validated the performance increase. Compared to conventional non-iterative methods, the IR-DCSK system provides increased efficiency and dependability, making it a viable option for reliable communication in difficult settings.

Utilizing Commutation Code Index (CCI) modulation to improve energy and spectral efficiencies, the research in [13] presented CCI-DCSK, a novel non-coherent modulation system. For the purpose of optimizing spectral efficiency, CCI-DCSK simultaneously transmits a reference sequence and its orthogonal data-bearing version within a single time slot. A commutated replica of the reference signal is mapped with additional bits to spread the modulated bit. The index

with the largest correlation magnitude was identified at the receiver through correlation with every conceivable commutated replica, allowing for precise bit estimation. Slightly better performance than current non-coherent chaotic modulation schemes is confirmed by the derivation of analytical BER expressions for multipath Rayleigh fading channels and AWGN.

In comparison to current techniques, Permutation Index DCSK (PI-DCSK), a novel non-coherent modulation scheme, has been introduced in [14] with the goal of improving data security, energy efficiency, and spectral efficiency. Every data frame in PI-DCSK is split into two time slots: first slot includes the reference chaotic signal while the second slot includes a permuted replica of the signal modulated by the data bits. At the transmitter,  $n + 1$  bits are grouped, where 1 bit modulates the permuted signal and  $n$  bits select a permutation of the reference signal. In order to decode data bits and retrieve the modulated signal, the receiver correlates received signals with every conceivable combination. In addition, a novel multiple access (MA) technique specifically designed for PI-DCSK is incorporated into the scheme. Its performance in single-user and multi-user scenarios over AWGN and multipath Rayleigh fading channels is examined. The promising performance of PI-DCSK in comparison to other non-coherent chaotic modulation schemes is confirmed by comparative analysis.

To improve Physical Layer Security (PLS) in OFDM-DCSK systems, [15] had introduced TRAN-OFDM-DCSK, a system that combines Time-Reversal (TR) pre-coding with Artificial Noise (AN) injection. Genuine receivers are unaffected by AN, but eavesdropper detection is compromised. It uses sender-only Channel State Information (CSI) to guarantee secure communication. With the use of simulation verification and derived BER expressions, performance under Flat Rayleigh Fading Channel (FRFC) was examined. Improved secrecy in both BER and SR metrics is validated by Ergodic Secrecy Rate (SR) analysis, which demonstrates better performance at real receivers than eavesdroppers.

In contrast to current Grouping Subcarrier Index-Modulation DCSK (GSIM-DCSK) techniques, the authors in [16] had presented Grouping Frequency-Time Index Modulation-DCSK (GFTIM-DCSK-I), a novel system designed to improve energy efficiency (EE), spectral efficiency, and data rates. GFTIM-DCSK-I divides data bits into  $L$  groups, each containing  $(P_1 + P_2 + 1)$  bits, in order to optimize frequency and time resources.  $P_1$  bits choose a subcarrier,  $P_2$  bits select a time slot, and one bit uses DCSK to modulate the signal within each group. In comparison to conventional DCSK, analytical expressions measure EE, spectral efficiency, and system complexity. The BER performance of the system is examined under multipath Rayleigh fading and AWGN, and simulations are used to verify the theoretical accuracy and better performance compared to traditional DCSK techniques.

An iterative receiver for M-ary DCSK modulation over AWGN channels is proposed in [17], which combined the decoding and demodulation to improve the performance through the exchange of extrinsic data. The optimal carrier syn-

chronization assumptions and efficient application of Log-Likelihood Ratios (LLRs) are credited with the simulation's superiority over noniterative approaches. Extrinsic information transfer charts also examined the convergence behavior, emphasizing enhanced efficiency and accuracy in decoding within the suggested receiver framework.

In discussing M-ary DCSK systems in the IoT, the work in [18] pointed out the shortcomings in conventional decoders and suggested an improved method. Using repeated chaotic signals for precise LLR computation and introduced the Initial Chaotic Signal Estimation (ICSE) algorithm. Furthermore, for better system performance, a unique protograph code with a P-EXIT algorithm is suggested. Competitiveness is demonstrated by analytical and simulated results, indicating that the M-ary protograph-coded DCSK with ICSE is a promising solution for low-complexity, low-power IoT devices.

Protograph-based LDPC (P-LDPC) codes has been introduced in [19], which is specifically designed for M-ary DCSK systems that use Iterative Receivers (IRs). Because of their interaction with soft information and chaotic carrier characteristics, conventional P-LDPC codes might not maximize the performance. To improve IR convergence, a new design principle including a finite-length Extrinsic Information Transfer (EXIT) algorithm has been introduced. The efficacy of the suggested P-LDPC codes is validated by analytical and simulated results, which emphasize their superiority in enhancing error correction for M-ary DCSK systems.

To the best of our knowledge, no studies have examined DCSK with index modulation using LDPC or New Radio-Polar Code (NRPC), which have been studied in the past for DCSK systems. The purpose of this work is to examine the possible advantages of using channel coding, specifically, LDPC and NRPC—in Grouping Subcarrier Index Modulation aided DCSK (GSIM-DCSK) systems in order to improve overall system performance. By using this method, we may investigate the benefits of integrating reliable error correction techniques with index modulation, which enhances communication systems' efficiency and dependability.

The contribution of this work is as follows:

- 1) The improved GSIM-DCSK using coded communication systems is investigated over multipath Rayleigh fading channel.
- 2) NRPC and P-LDPC codes are used to enhance the performance of GSIM-DCSK over multipath Rayleigh fading channel.
- 3) The simulations are performed using MATLAB and the results are compared with coded OFDM-DCSK system.

This work is organized as follows; Sections II and III illustrate the coding techniques used, Section IV presents the system model for this work, Sections V and VI show the simulation results and discuss the results with complexity calculations. Finally, Section VII concludes this work.

## II. POLAR CODE

The implementation of an error control code based on channel polarization [20] has successive cancellation approaching capacity. When M polarized channels approach infinity with

codeword length  $\mu$ , two distinct results emerge: noiseless channels and nearly fully noisy channels. While frozen bits are transmitted through noiseless channels, information bits are distributed throughout channels with pure noise during the encoding process. Data vector  $S_1^\mu = (S_1, S_2, \dots, S_\mu)$  contains the information.  $R = \frac{J}{\mu}$  is the coding rate, and  $S_A$  represents the J-bit information. The remaining bits are frozen and are represented as  $S_{A^c}$ . This is the form of the codeword:

$$S_1^\mu = S_1^\mu G_\mu = S_1^\mu B_\mu F_2^{\otimes m} \quad (1)$$

where  $G_\mu$  is the generator matrix,  $B_\mu$  is the bit reversal permutation matrix and  $F_2^{\otimes m}$  represent the  $m$ th Kronecker power of  $F_2$ , where  $F_2$  represents the kernel matrix such that:

$$F_2 = \begin{bmatrix} 1 & 0 \\ 1 & 1 \end{bmatrix} \quad (2)$$

The successive cancellation (SC) decoder at the receiver generates  $\hat{S}_1^\mu$  as an estimation of  $S_1^\mu$  by observing  $(y_1^\mu, S_{A^c})$  and the likelihood ratio (LR)  $L_\mu^{(i)}(y_1^\mu, \hat{S}_1^{i-1})$  is calculated using

$$L_\mu^{(i)}(y_1^\mu, \hat{S}_1^{i-1}) = \frac{W_\mu^{(i)}(y_1^\mu, \hat{S}_1^{i-1} | 0)}{W_\mu^{(i)}(y_1^\mu, \hat{S}_1^{i-1} | 1)} \quad (3)$$

where  $W_\mu^{(i)}(y_1^\mu, \hat{S}_1^{i-1} | \gamma)$  is the noise probability where  $\gamma$  is 0 or 1 and the decision can be calculated from:

$$\hat{S}_i = \begin{cases} S_i, & i \in A^c \\ h_i(y_1^\mu, \hat{S}_1^{i-1}), & i \in A \end{cases} \quad (i = 1, 2, 3, \dots, \mu) \quad (4)$$

and

$$h_i(y_1^\mu, \hat{S}_1^{i-1}) = \begin{cases} 0, & L_\mu^{(i)}(y_1^\mu, \hat{S}_1^{i-1}) \geq 1 \\ 1, & \text{otherwise} \end{cases} \quad (5)$$

where, the decision function  $h_i$  is used in the succeeding decision elements (DEs), the LR is calculated based on equations (6) and (7):

$$L_\mu^{(2i-1)}(y_1^\mu, \hat{S}_1^{2i-2}) = f\left(L_{\mu/2}^{(i)}(y_1^{\mu/2}, \hat{S}_{1,o}^{2i-2} \oplus \hat{S}_{1,e}^{2i-2}), L_{\mu/2}^{(i)}(y_{\mu/2+1}^\mu, \hat{S}_{1,e}^{2i-2})\right) \quad (6)$$

$$L_\mu^{(2i)}(y_1^\mu, \hat{S}_1^{2i-1}) = g\left(L_{\mu/2}^{(i)}(y_1^{\mu/2}, \hat{S}_{1,o}^{2i-2} \oplus \hat{S}_{1,e}^{2i-2}), L_{\mu/2}^{(i)}(y_{\mu/2+1}^\mu, \hat{S}_{1,e}^{2i-2}), \hat{S}_{2i-1}\right) \quad (7)$$

where  $f(a, b)$  and  $g(a, b, \hat{S}_{sum})$  are calculated using equations (8) and (9), respectively

$$f(a, b) = \frac{1 + ab}{a + b} \quad (8)$$

$$g(a, b, \hat{S}_{sum}) = a^{1-2\hat{S}_{sum}} b \quad (9)$$

where,  $a, b$  and  $\hat{S}_{sum}$  are defined as follows

$$a = L_{\mu/2}^{(i)}(y_1^{\mu/2}, \hat{S}_{1,o}^{2i-2} \oplus \hat{S}_{1,e}^{2i-2}) \quad (10)$$

$$b = L_{\mu/2}^{(i)}(y_{\mu/2+1}^\mu, \hat{S}_{1,e}^{2i-2}) \quad (11)$$

$$\hat{S}_{sum} = \hat{S}_{2i-1} \quad (12)$$

The modified SC decoding algorithm is the successive cancellation list (SCL) decoding algorithm that is introduced in [21] in which, the decoder is duplicated in two parallel decoding threads continuing in either possible direction. The number of parallel decoding threads is denoted by  $L$  and the algorithm of SCL decoding is summarized in [22].

### III. LOW-DENSITY PARITY-CHECK (LDPC) CODE

Binary  $(E, K)$  LDPC code is a type of Linear Block Code (LBC) described by a bipartite graph and constructed from a  $(E - K) \times E$  parity-check matrix  $H$  with low density of 1s. The matrix  $H$  has two types of Nodes:  $E$  symbol nodes that is designated by  $u$  and represent the encoded symbols, while  $(E - K)$  parity check nodes are designated by  $v$  and represent the parity checks [23]. An edge connector is used to link check node and symbol nodes. The 5G New Radio (NR) LDPC is the most familiar mark for the 3rd Generation Partnership Project (3GPP) of cellular technologies [24]. It has two rate-compatible base graphs (BGs), BG1 and BG2, for the LDPC code. BG1 utilizes large block length ( $500 \leq K \leq 8448$ ) and higher code rates ( $\frac{1}{3} \leq \text{Code rate} \leq \frac{8}{9}$ ), BG2 utilizes shorter block ( $40 \leq K \leq 2560$ ) and lower code rates ( $\frac{1}{5} \leq \text{Code rate} \leq \frac{2}{3}$ ).

For a BG,  $k_b$  and  $n_b$  are used to represent the corresponding BG parameters. Nominally, if the lifting value is  $Z$ , we have the input data block size  $K = Z \times k_b$  and the code block (CB) size  $N = Z \times n_b$  as mentioned in [25]. The total lifting set  $Z$  is set from the minimum value 2 to the maximum value 384 according to  $Z = A \times 2^j$ , where  $A = 2, 3, 5, 7, 9, 11, 13, 15$  and  $j = 0, 1, \dots, 7$ . In our work, BG1 is used to construct the parity check matrix  $H$ . A BG1 matrix example is shown in Fig. 1. There are five zones in the matrix: A, B, C, D, and O. Core information columns are represented by zone A, core parity checks are introduced by zone B, and extension checks of zones A and B are provided by zones C, D and O. D is an identity matrix and O is a zero matrix. Two information columns in zone A will be pierced prior to the transmission in accordance to the 5G specification [25]. 5G LDPC codes employ shortening and puncturing techniques to accommodate different information lengths and rate adaption. While shortening is only intended via zero-padding for the information bits, punctuation is applied to both the information and parity bits in the codeword. In the LDPC encoder, the encoded codeword  $C$  is related to the  $H$  matrix according to [24]:  $\mathbf{HC}^T = \mathbf{0}^T$ , where  $T$  is the transpose operator. In the decoder, belief propagation (BP) iterative algorithm [23] is used to recover the original transmitted bits. Define  $Q_{uv}$  as the message passing from a  $u$  to  $v$  and  $R_{vu}$  as the message passing from a  $v$  to  $u$ . The log-likelihood-ratio (LLR) domain is used to describe the LDPC decoding algorithm. Let us define  $P_u = \log \frac{p_u(0)}{p_u(1)}$  as the log ratio of the transmitted bit probability of  $u$  is 0,  $p_u(0)$ , to the transmitted bit probability  $u$  is 1,  $p_u(1)$ . In BP, the messages from the  $u$  to the  $v$  are:

$$Q_{uv} = P_u + \sum_{\hat{v} \in N(u) \setminus v} R_{\hat{v}u}, \quad (13)$$

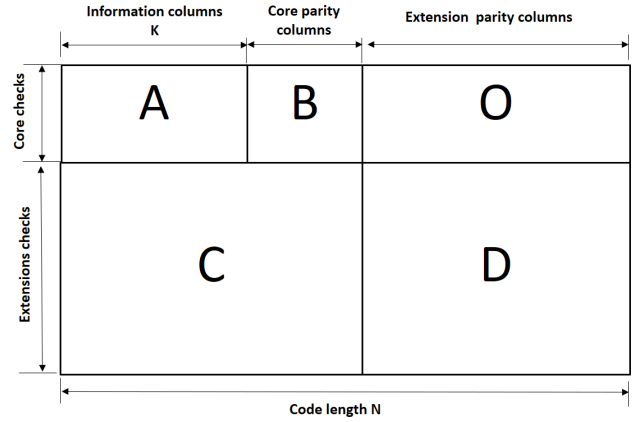


Fig. 1. Standard LDPC's base matrix.

where  $N(\cdot)$  is the set of neighboring nodes in the graph and the symbol  $\hat{v} \in N(u) \setminus v$  refers to  $\hat{v}$  belong to  $N(u)$  excluding  $v$  index. The messages from the  $v$  to the  $u$  are:

$$R_{vu} = 2 \tanh^{-1} \left( \prod_{\hat{u} \in N(v) \setminus u} \tanh \left( \frac{Q_{\hat{u}v}}{2} \right) \right) \quad (14)$$

While the soft decoding result for each symbol  $u$  is calculated as

$$Q_u = P_u + \sum_{v \in N(u)} R_{vu} \quad (15)$$

and the recovered binary bits  $b_u$  can be calculated from:

$$b_u = \begin{cases} 0, & \text{sign}(Q_u) < 0 \\ 1, & \text{sign}(Q_u) \geq 0 \end{cases} \quad (16)$$

### IV. CODED GSIM-DCSK SYSTEM MODEL

The transmitter structure of the CGSIM-DCSK system is illustrated in Fig. 2. Firstly, either the  $K$ -length data bits  $b$  are encoded by the NRPC at position-1 or LDPC code at position-2 into  $E$ -length coded bits  $c$ . The proposed systems are referred as NRPC-GSIM-DCSK and LDPC-GSIM-DCSK, respectively, and hence, the coded bits are modulated by a GSIM-DCSK system. In addition, two GSIM-DCSK schemes are used in our work that are GSIM-DCSK1 and GSIM-DCSK2, respectively as described in details in [26]. The coded bits are divided into  $G$  groups, each group has  $p_1$  bits assigned as subcarrier indexed bits and  $p_2$  bits assigned as modulated bits. The modulated bits  $p_2 = 1$  for CGSIM-DCSK1 and  $p_2 = (2^{p_1} - 1)$  for CGSIM-DCSK2, where the data is carried by active subcarrier. The total transmitted bits are  $p = G(p_1 + p_2)$ .

The reference chaotic signal  $x_k$  of length  $\beta$  is generated by a second-order Chebyshev polynomial function and filtered by a pulse-shaping filter to produce  $x_v(t)$  at the  $v$ th symbol period [26]. In each group the indexed bits are converted into index symbol,  $\delta_v^i$ , which is used to select one subcarrier in that group to generate the  $v$ th signal  $d_{v,j}^i, j = 1, \dots, 2^{p_1}$ ,  $i = 1, \dots, G$ . The signal  $d_{v,j}^i$  either contains the converted of the modulated bits  $\pm 1$  if the subcarrier is active, or set

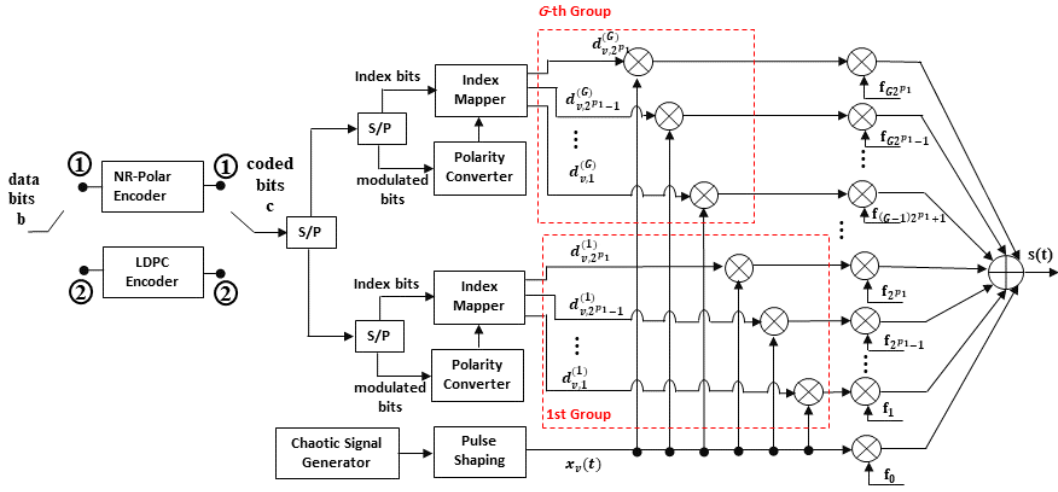


Fig. 2. Transmitter structure of the CGSIM-DCSK system.

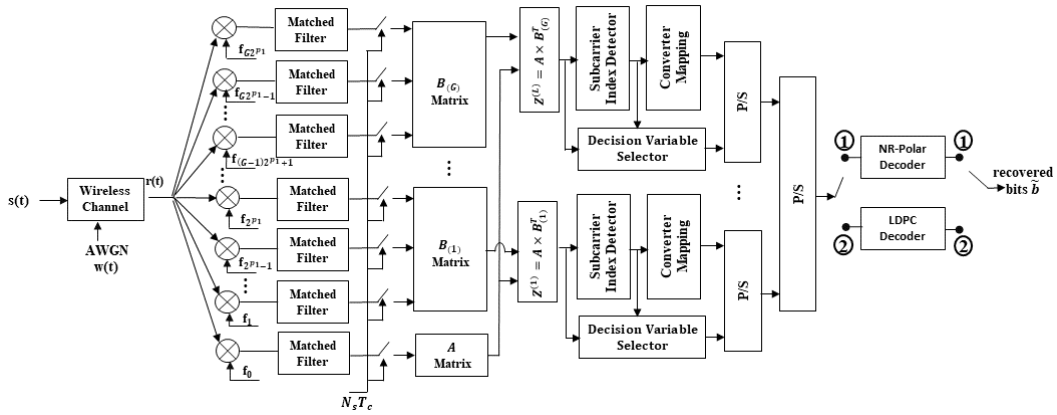


Fig. 3. Receiver structure of the CGSIM-DCSK system.

to zero for inactive subcarrier. After that, the signal  $d_{v,j}^i$  is multiplied by the reference chaotic signal, and all signals are then multiplexed using the multicarrier technique to generate the transmitted signal  $s(t)$  that is expressed as:

$$S(t) = \sum_{i=1}^G \sum_{j=1}^{2^{p1}} d_{v,j}^i \cos(2\pi f_{(i-1)2^{p1}+j} t + \phi_{(i-1)2^{p1}+j}) + x_v(t) \cos(2\pi f_0 t + \phi_0) \quad (17)$$

where  $f_{i,j}$  and  $\phi_{i,j}$  are the  $i$ th group and  $j$ th subcarrier of the center frequency and phase angle, respectively. There are  $N_s = 2^q + 1$  subcarriers, where  $q$  is an integer number greater than or equal to  $p_1$ , one of which sends the signal  $x_v(t)$  and the remaining are grouped into  $G$  group  $2^{q-p_1}$  each with  $2^{p_1}$  subcarriers.

The receiver structure of the CGSIM-DCSK system is illustrated in Fig. 3. The received signal is achieved by passing the transmitted signal through multipath Rayleigh fading channel and summing by AWGN signal  $w(t) \in \mathcal{N}(0, N_0/2)$  and can be expressed as:

$$r(t) = \sum_{l=1}^{\Gamma} \alpha_l S(t - \tau_l) + w(t), \quad (18)$$

Where  $\Gamma$  is the total number of paths, and  $\tau_l$  and  $\alpha_l$  are the  $l$ th delay and coefficient of the channel. The  $\alpha_l$  values are assumed to be independent Rayleigh distribution random variable. For simplicity, only the first symbol period is considered and  $v$  is removed from the next equations.

The reception signal is mixed by the corresponding sinusoidal subcarrier synchronized with the sending side and followed by a matched filter. Algorithm 1 shows the effective detection algorithm to recover the sending bits. Let us define  $\mathbf{A}_{1 \times \beta}$  and  $\mathbf{B}_{2^{p1} \times \beta}^i$ ,  $i = 1, \dots, G$ , the matrices containing the collection of the reference chaotic signal and the  $i$ th information carrying signal, respectively. Then, the  $i$ th correlation matrices  $\mathbf{Z}^i$ ,  $i = 1, \dots, G$ , can be expressed as

$$\mathbf{Z}^i = \mathbf{A} \times (\mathbf{B}^i)^T = [z_1^i z_2^i, \dots, z_{2^{p1}}^i]^T \quad i = 1, \dots, G \quad (19)$$

**Algorithm 1** Proposed CGSIM–DCSK Receiver Algorithm

- 
- 1: Input:  $r_{\sigma,k}, r_{i,j,k}, i = 1, \dots, 2^{p_1}, k = 1, \dots, \beta, m = 1, \dots, p_1, E, n = 1, \dots, p_2, sel$ .
  - 2: Output: detected bits  $\hat{b}$ .
  - 3: For  $i \leftarrow 1 : G$
  - 4: Calculate the decision variables at the output of the  $j$ th correlator by Eq. (19),  $z_{i,j}, j = 1, \dots, 2^{p_1}$ .
  - 5: Calculate the  $i$ th estimated subcarrier index by Eq. (20),  $\hat{\delta}_i$ .
  - 6: Convert  $\hat{\delta}_i$  to binary sequence  $\delta_{i,m}^{\hat{}} = \{\delta_{i,1}^{\hat{}}, \dots, \delta_{i,p_1}^{\hat{}}\}$ .
  - 7: Map each bit to bipolar symbol  $\delta_{i,m}^{\hat{}} = 2\delta_{i,m}^{\hat{}} - 1$ .
  - 8: Calculate the soft modulated bit by Eq. (21),  $a_n^i$ .
  - 9: Calculate the input likelihood ratio soft bits according Eq. (22).
  - 10: end  $i$  loop.
  - 11: calculate  $\hat{b}$ ,
  - 12: **if**  $sel = 1$  **then**
  - 13:    $\hat{b} = \text{NR-POLAR-Decoder(LLR)}$
  - 14: **else**
  - 15:    $\hat{b} = \text{LDPC-Decoder (LLR)}$ .
- 

For both systems, the estimated subcarrier index in the  $i$ th group is detected using the following expression:

$$\hat{\delta}_i = \begin{cases} \arg \max_{j=1, \dots, 2^{p_1}}, & \text{for CGSIM-DCSK1} \\ \arg \min_{j=1, \dots, 2^{p_1}}, & \text{for CGSIM-DCSK2} \end{cases} \quad i = 1, \dots, G \quad (20)$$

The estimate subcarrier indices select the soft decision variables at the  $i$ th group according to:

$$a_n^i = \begin{cases} z_{\hat{\delta}_i}^i, j = \hat{\delta}_i, & \text{for CGSIM-DCSK1} \\ z_j^i, j = 1, \dots, 2^{p_1}, j \neq \hat{\delta}_i, & \text{for CGSIM-DCSK2} \end{cases} \quad (21)$$

for  $n = 1, \dots, p_2$ . The estimated subcarrier index is converted into binary sequence of the estimated index bits,  $\delta_{i,m}^{\hat{}} = \{\delta_{i,1}^{\hat{}}, \dots, \delta_{i,p_1}^{\hat{}}\}$ . Each bit in  $\delta_{i,m}^{\hat{}}$  is mapped to  $\pm 1$  according to its polarity to get the soft value of the index bits,  $2\delta_{i,m}^{\hat{}} - 1$ . After that, the soft decision variables  $a_j^i$  and the symbol of the index bits for each group are concatenated to obtain the LLR vector according to:

$$LLR_{(i-1)p+o} = -[\delta_{i,1}^{\hat{}}, \dots, \delta_{i,p_1}^{\hat{}}, a_1^i, \dots, a_{p_2}^i], \quad o = 1, \dots, p. \quad (22)$$

After that, the soft bits are ready to enter to the channel decoder stage. At the decoder stage, the soft bits are passed either at position–1 in the case of the NRPC–GSIM–DCSK system or at position–2 in the case of the LDPC–GSIM–DCSK system.

## V. SIMULATION RESULTS AND DISCUSSION

To demonstrate the effectiveness of coding modulation in improving the GSIM–DCSK communication system, this section examines the MATLAB simulation results. The average

power gain and time delays of the three path fading channels are set to ( $\alpha_1 = \alpha_2 = \alpha_3 = 1/3$ ) and ( $\tau_1 = 0, \tau_2 = 1, \tau_3 = 2$ ), respectively. The spreading factor is set to  $\beta = 100$  and  $200$ . The NR–Polar and LDPC code rates are set to  $(1/2, 1/3)$ . Figs. 4 and 5 show the comparison of the LDPC–GSIM–DCSK system with the LDPC–OFDM–DCSK system over a three–path Rayleigh fading channel and different code rates for  $\beta = 100$  and  $200$ , respectively. The performance of both systems are improved compared to uncoded systems, for instance, the coding gain for Scheme 1 at  $\beta = 100$  and  $\text{BER} = 10^{-3}$  are about 7 dB and 8 dB for the code rate  $1/2$  and  $1/3$  respectively. Furthermore, the performance of both systems improved when the code rate is reduced. At  $\beta = 100$  and  $\text{BER} = 10^{-3}$ , the code gain of  $1/3$  rate compared to  $1/2$  is 2.5 dB and 4 dB for LDPC–GSIM–DCSK1 and for LDPC–GSIM–DCSK2, respectively. However, increasing the spreading factor leads to a deterioration in the performance of both systems. To illustrate that, for LDPC–GSIM–DCSK1 at code rate =  $1/2$  and  $\text{BER} = 10^{-3}$ , the coding gain of  $\beta = 100$  compared to  $200$  is 3 dB.

Furthermore, LDPC–GSIM–DCSK1 outperforms LDPC–GSIM–DCSK2 in all cases, for example, at  $\beta = 100$  and  $\text{BER} = 10^{-3}$ , the coding gain of Scheme 1 compared to Scheme 2 is 2.5 dB and 1 dB for code rate  $1/2$  and  $1/3$ . Furthermore, the performance of both proposed systems exceeds that of the traditional coded OFDM–DCSK system. For code rate  $1/2$  and  $\text{BER} = 10^{-3}$ , there is a coding gain of about 1.5 dB and 3.5 dB compared to LDPC–OFDM–DCSK for LDPC–GSIM–DCSK1 and LDPC–GSIM–DCSK2, respectively. Similarly, code rate  $1/3$  results in a coding gain of approximately 3.5 dB and 5 dB for Scheme 1 and Scheme 2, respectively.

Simulation results of NRPC–GSIM–DCSK systems for the spreading factor  $\beta = 100$  and  $200$  are shown in Figs. 6 and 7, respectively. That show the performance of both systems decreases when the spreading factor is increased. Furthermore, reducing the code rate will improve the performance of the systems as shown for NRPC–GSIM–DCSK1 and NRPC–GSIM–DCSK2 at  $\beta = 100$  and  $\text{BER} = 10^{-4}$ , where the coding gain of code rate  $1/3$  compared to code rate  $1/2$  are 2.5 dB and 3 dB, respectively. By comparing the performance of NRPC with LDPC on both systems, it can be observed that LDPC outperforms the performance of NRPC.

Fig. 8 shows the BER performance of LDPC–GSIM–DCSK1 for various delay times and spreading factors. It is evident that the performance is degraded when the delay is increased, but this degradation is evident when  $\beta$  is small. Furthermore, increasing the spreading factor will degrade the performance of the system.

Fig. 9 compares the BER performance of the proposed systems LDPC–GSIM–DCSK1 and LDPC–GSIM–DCSK2 with the LDPC–Mary–DCSK from [19] under AWGN channel. It is evident that the performance of LDPC–GSIM–DCSK1 outperforms LDPC–Mary–DCSK, however, LDPC–GSIM–DCSK2 has the lowest BER performance. For instance, at  $\text{BER} = 10^{-5}$  the LDPC–GSIM–DCSK1 system achieves SNR gain about 1 dB better than the LDPC–Mary–DCSK system for the

same code rate and  $\beta$  values. The increased number of modulating bits carried by the GSIM-DCSK2 system increases the data rate on the consequences of degrading the performance in comparison to the GSIM-DCSK1 system.

## VI. COMPLEXITY COMPUTATION

The complexity of GSIM-DCSK1 and GSIM-DCSK2 is calculated in detail in [26]. The multiplication of the transmitter and the receiver for both systems as a function of  $q$  are  $2^{q+1} + 1$  and  $2(2^q + 1) + 2^q$ , respectively. In addition, LDPC codes and Polar codes each have a specific computational complexity. Although, LDPC codes are known for their effective error correction capabilities, the decoding process typically requires more computing power of  $O(IN)$ , where  $I$  is the number of iterations needed and  $N$  is the length of the codeword. Conversely, polar codes use structured transformations to provide effective error correction, making them suitable for 5G communication applications. Its decoding complexity is  $O(N \log(N))$  and can be achieved through the use of algorithms such as SC. For spread spectrum communication, DCSK modulation uses chaotic sequences and carrying out modulation and demodulation operations which both have  $O(N)$  complexity. These methods demonstrate different trade-offs between computational complexity and performance. DCSK modulation provides effective spread spectrum capabilities through chaotic waveforms, balancing computational efficiency with signal robustness in noisy environments like wireless communications and secure data transmission protocols. LDPC and Polar codes offer robust error correction at the cost of higher computational overhead.

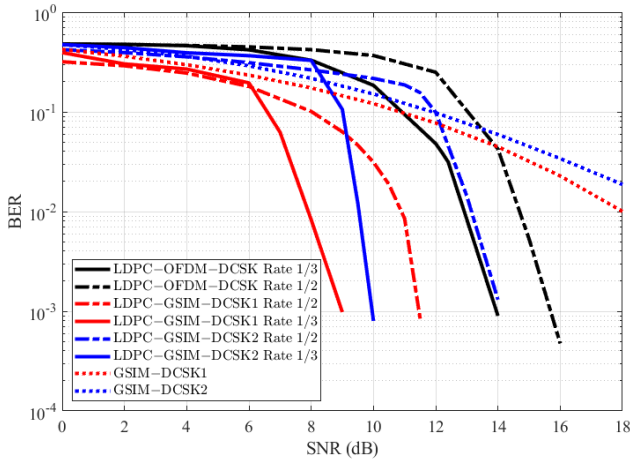


Fig. 4. BER plot of the LDPC-GSIM-DCSK1 and LDPC-GSIM-DCSK2 systems with various coding rates and at  $\beta = 100$ , the block size is  $N = 2048$  and the number of iterations is 20.

## VII. CONCLUSION

This article presents a study on the performance of NRPC and LDPC code-based GSIM-DCSK systems. Different code rates, spreading factors and list numbers are compared for GSIM-DCSK1 and GSIM-DCSK2 systems. In the proposed

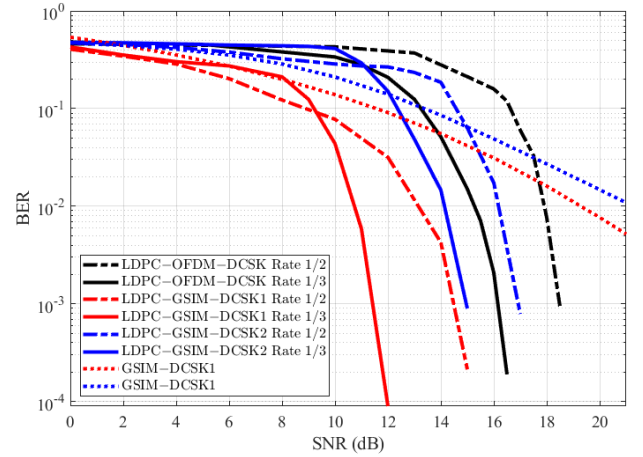


Fig. 5. BER plot of the LDPC-GSIM-DCSK1 and LDPC-GSIM-DCSK2 systems with various coding rates and at  $\beta = 200$ , the block size is  $N = 2048$  and the number of iterations is 20.

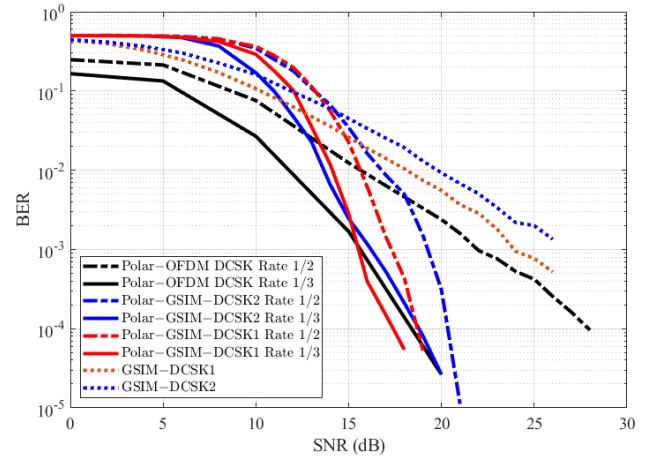


Fig. 6. BER plot of the NRPC-GSIM-DCSK1 and NRPC-GSIM-DCSK2 systems with various coding rates and at  $\beta = 100$ .

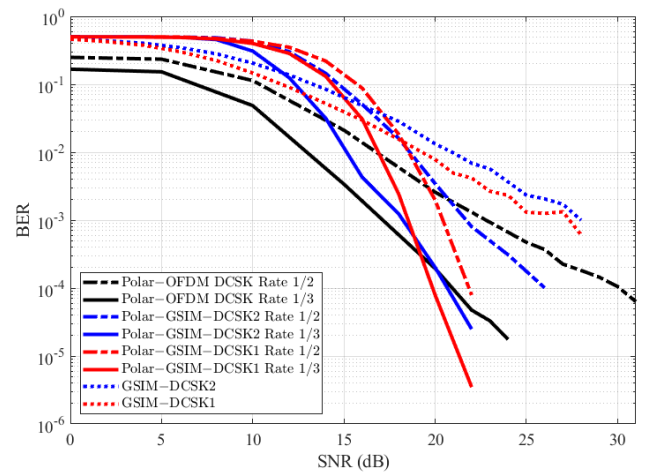


Fig. 7. BER plot of the NRPC-GSIM-DCSK1 system with various  $\beta = 50, 100, 200$  and various code rate.

method, all index modulation bits are demodulated and con-

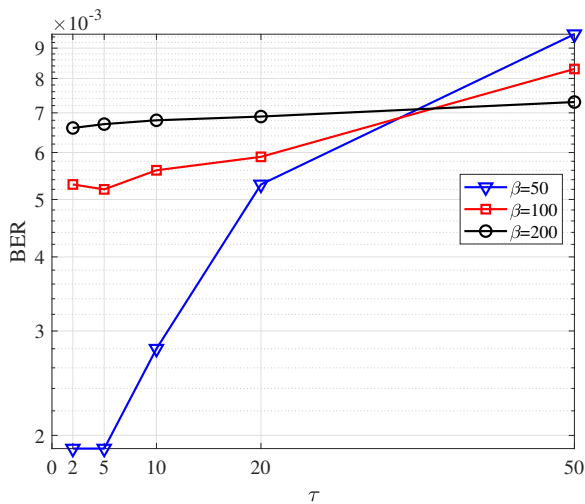


Fig. 8. BER plot of the LDPC-GSIM-DCSK1 system versus delay  $\tau$  with various  $\beta = 50, 100, 200$ . The time delays of three paths are  $\tau_1 = 0$ ,  $\tau_2 = \tau$ , and  $\tau_3 = 2\tau$ . The rate  $= 1/3$ ,  $N=1024$ , and  $\text{SNR}=5$  dB.

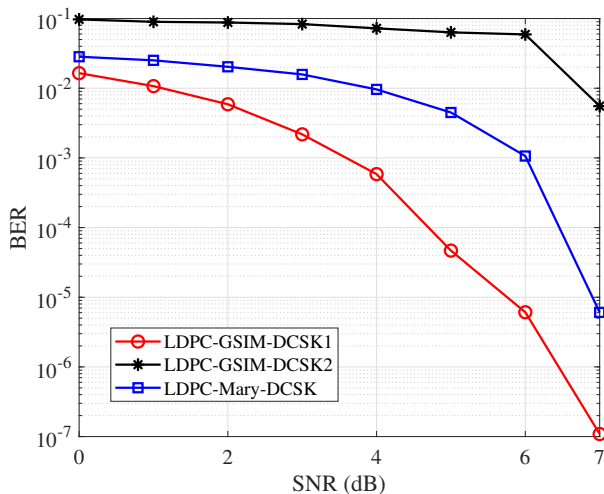


Fig. 9. AWGN channel performance comparison between proposed systems and LDPC-Mary-DCSK system [19]. The simulation parameters are  $\beta = 20$ , code rate  $= 2/3$ ,  $M = 16$ , and  $N = 1024$ .

verted into a bipolar form to pass them through the decoded system along with the soft modulated bits. The result shows that the coded systems outperform the uncoded systems and the reliability of both systems is improved. Additionally, increasing the spreading factor affects the performance of both systems, and the performance of the systems is improved when the code rate is reduced. The results show that the performance of LDPC code at large block length outperforms that of NR-Polar at high complexity. In addition, the performance of CGSIM-DCSK systems is better than that of the traditional coded OFDM-DCSK modulation system.

## REFERENCES

- [1] F. C. M. Lau and C. K. Tse, *Chaos-based digital communication systems: operating principles, analysis methods, and performance evaluation*. Springer Publishing Company, Incorporated, 2011.
- [2] M. Kennedy, G. Kolumban, G. Kis, and Z. Jako, "Performance evaluation of FM-DCSK modulation in multipath environments," *IEEE Transactions on Circuits and Systems I: Fundamental Theory and Applications*, vol. 47, no. 12, pp. 1702–1711, 2000.
- [3] G. Kolumban, M. Kennedy, Z. Jako, and G. Kis, "Chaotic communications with correlator receivers: theory and performance limits," *Proceedings of the IEEE*, vol. 90, no. 5, pp. 711–732, 2002.
- [4] G. Kolumban, "Theoretical noise performance of correlator-based chaotic communications schemes," *IEEE Transactions on Circuits and Systems I: Fundamental Theory and Applications*, vol. 47, no. 12, pp. 1692–1701, 2000.
- [5] W. Xu and L. Wang, "CIM-DCSK: A differential chaos shift keying scheme with code-index modulation," in *2016 16th International Symposium on Communications and Information Technologies (ISCIT)*, 2016, pp. 100–104.
- [6] P. Chen, L. Shi, Y. Fang, G. Cai, L. Wang, and G. Chen, "A coded DCSK modulation system over Rayleigh fading channels," *IEEE Transactions on Communications*, vol. 66, no. 9, pp. 3930–3942, 2018.
- [7] Y. Fang, J. Zhuo, H. Ma, S. Mumtaz, and Y. Li, "Design and analysis of a new index-modulation-aided DCSK system with frequency-and-time resources," *IEEE Transactions on Vehicular Technology*, vol. 72, no. 6, pp. 7411–7425, 2023.
- [8] H. Yang and G.-P. Jiang, "Reference-modulated DCSK: A novel chaotic communication scheme," *IEEE Transactions on Circuits and Systems II: Express Briefs*, vol. 60, no. 4, pp. 232–236, 2013.
- [9] W. Xu, L. Wang, and G. Chen, "Performance analysis of the CS-DCSK/BPSK communication system," *IEEE Transactions on Circuits and Systems I: Regular Papers*, vol. 61, no. 9, pp. 2624–2633, 2014.
- [10] G. Cai, Y. Fang, J. Wen, S. Mumtaz, Y. Song, and V. Frascolla, "Multi-carrier  $M$ -ary DCSK system with code index modulation: An efficient solution for chaotic communications," *IEEE Journal of Selected Topics in Signal Processing*, vol. 13, no. 6, pp. 1375–1386, 2019.
- [11] W. Xu, T. Huang, and L. Wang, "Code-shifted differential chaos shift keying with code index modulation for high data rate transmission," *IEEE Transactions on Communications*, vol. 65, no. 10, pp. 4285–4294, 2017.
- [12] Y. Lyu, L. Wang, G. Cai, and G. Chen, "Iterative receiver for  $M$ -ary DCSK systems," *IEEE Transactions on Communications*, vol. 63, no. 11, pp. 3929–3936, 2015.
- [13] M. Herceg, D. Vranješ, G. Kaddoum, and E. Soujeri, "Commutation code index DCSK modulation technique for high-data-rate communication systems," *IEEE Transactions on Circuits and Systems II: Express Briefs*, vol. 65, no. 12, pp. 1954–1958, 2018.
- [14] M. Herceg, G. Kaddoum, D. Vranješ, and E. Soujeri, "Permutation index DCSK modulation technique for secure multiuser high-data-rate communication systems," *IEEE Transactions on Vehicular Technology*, vol. 67, no. 4, pp. 2997–3011, 2018.
- [15] D. H. Hameed and F. S. Hasan, "Physical layer security using time-reversal pre-coding based OFDM-DCSK communication system with artificial noise injection," *Journal of Communications Software and Systems*, vol. 19, no. 4, pp. 289–298, 2023.
- [16] R. A. Yaseen and F. S. Hasan, "Design and analysis of grouping active subcarrier frequency-time index modulation for differential chaos shift keying communication system," *Journal of Communications Software and Systems*, vol. 20, no. 2, pp. 173–185, 2024.
- [17] Y. Lyu, G. Cai, and L. Wang, "Iterative demodulation and decoding of LDPC-coded  $M$ -ary DCSK modulation over AWGN channel," in *2014 8th International Symposium on Medical Information and Communication Technology (ISMICT)*, 2014, pp. 1–5.
- [18] Y. Li, L. Dai, and L. Lv, "Design of an improved  $M$ -ary DCSK-aided protograph-coded communication system," *IEEE Access*, vol. 11, pp. 55 002–55 010, 2023.
- [19] Q. Chen, L. Wang, Y. Lyu, and G. Chen, "Designing protograph-based LDPC codes for iterative receivers on  $M$ -ary DCSK systems," *IEEE Transactions on Circuits and Systems II: Express Briefs*, vol. 65, no. 4, pp. 466–470, 2018.
- [20] E. Arıkan, "Channel polarization: A method for constructing capacity-achieving codes for symmetric binary-input memoryless channels," *IEEE Transactions on Information Theory*, vol. 55, no. 7, pp. 3051–3073, 2009.
- [21] I. Tal and A. Vardy, "List decoding of polar codes," *IEEE Transactions on Information Theory*, vol. 61, no. 5, pp. 2213–2226, 2015.
- [22] A. Balatsoukas-Stimming, M. B. Parizi, and A. Burg, "LLR-based successive cancellation list decoding of polar codes," *IEEE Transactions on Signal Processing*, vol. 63, no. 19, pp. 5165–5179, 2015.

- [23] E. Sharon, S. Litsyn, and J. Goldberger, "An efficient message-passing schedule for LDPC decoding," in *2004 23rd IEEE Convention of Electrical and Electronics Engineers in Israel*, 2004, pp. 223–226.
- [24] T. T. B. Nguyen, T. Nguyen Tan, and H. Lee, "Efficient QC-LDPC encoder for 5G new radio," *Electronics*, vol. 8, no. 6, 2019. [Online]. Available: <https://www.mdpi.com/2079-9292/8/6/668>
- [25] A.-H. C. (Nokia), "Chairman's notes of agenda item 7.1. 4. channel coding. 3GPP TSG RAN WG1 meeting AH 2, R1-1711982," 2017.
- [26] F. S. Hasan, "Design and analysis of grouping subcarrier index modulation for differential chaos shift keying communication system," *Physical Communication*, vol. 47, p. 101325, 2021. [Online]. Available: <https://www.sciencedirect.com/science/article/pii/S1874490721000628>



**Ali Jaber Al-Askery** is an assistant professor in the Electrical Engineering Technical College-Middle Technical University, Baghdad, Iraq. He received the B.Sc. and M.Sc. degrees in Electrical Engineering from Al-Mustansiriyah University, Baghdad, Iraq, in 2001 and 2004, respectively. He received his PhD from the School of Electrical and Electronics Engineering, Newcastle University, Newcastle Upon Tyne, U.K. His research focuses on wireless communications, wired communications, OFDM systems, coded systems and receiver design.



**Fadhil Sahib Hasan** was born in Baghdad, Iraq in 1978. He received his B.Sc. degree in Electrical Engineering in 2000 and his M.Sc. degree in Electronics and Communication Engineering in 2003, both from the Mustansiriyah University, Iraq. He received Ph.D. degree in 2013 in Electronics and Communication Engineering from the Basrah University, Iraq. In 2005, he joined the Faculty of Engineering at the Mustansiriyah University in Baghdad. His recent research activities cover wireless communication systems, multicarrier systems,

wavelet based OFDM, MIMO systems, speech signal processing, chaotic modulation, FPGA and Xilinx system generator based communication systems. Since 2022, he has been a professor at the Mustansiriyah University, Iraq.



**Ahmed A. Thabit** currently works at the department of Communication Engineering, Al Rafidain University College from 2008 to 2023, at now he is Professor at the Middle Technical University. Ahmed does research in Electronic Communication Engineering. Their current project is 'Design and simulation of adaptive equalizer for RF systems.